# RSC Advances

## PAPER

# Organic sodium terephthalate@graphene hybrid anode materials for sodium-ion batteries†

Ying Wang, Katja Kretschmer, Jinqiang Zhang, Anjon Kumar Mondal, Xin Guo and Guoxiu Wang*

In the search for high-performance electrodes for sodium-ion battery applications, there is a high demand for organic materials with satisfactory electrochemical performances, especially high rate capabilities. Herein, we report an organic based composite, sodium terephthalate@graphene ($Na_2TP@GE$) hybrid synthesized *via* freeze-drying technique. This material shows an interconnected, multi-channelled monolith structure, which resulted in outstanding rate capability for sodium storage. This hybrid material demonstrated a high reversible capacity of 268.9 mA h $g^{-1}$ and prolonged cyclability with capacity retention of 77.3% over 500 cycles.

## Introduction

As the most promising alternative candidates for the next generation battery systems, rechargeable sodium-ion (Na-ion) batteries have gained great interest over the last few years.[1-3] Conventionally, anode materials for Na-ion batteries include carbonaceous materials, metal oxides and phosphates, and alloys.[4] However, unlike commercialized carbonaceous materials in lithium-ion (Li-ion) battery systems, sodium atoms barely intercalate into graphitic carbons.[5,6] In addition, the use of metal oxides and metal alloys as electrode materials is far from renewable, not to mention the sluggish intercalation of sodium and extremely poor cyclability in the case of Si, Ge, Sb and Bi *etc.*[7-10] Therefore, intensive efforts have been made in searching for suitable organic materials that possess the advantages of electrochemical activity and natural abundance, while being environment-friendly, which make the concept of clean energy possible.

The first small-molecule based organic electrode was reported by D. L. Williams in 1969,[11] followed by extensive investigations on lithium-containing carbonyl-based organics,[12,13] carboxylate,[14-16] oxocarbons,[17,18] and poly-ketones.[19,20] Na-ion battery operation resembles the reaction mechanism of Li-ion batteries and the potential difference between lithium and sodium metal is only 0.3 V, suggesting the feasibility and availability of organic materials for Na-ion batteries. For instance, K. Amine's group surveyed a series of organic carboxylate based materials as the anode materials for

Na-ion batteries.[21] They exhibited a long discharge plateau below 0.6 V *vs.* Na/Na$^+$. Jun Chen's group investigated the electrochemical performance of $Na_4C_8H_4O_4$, which can be used as both positive and negative electrode material in Na-ion batteries.[22] Furthermore, Yong Lei's group reported several conjugated organic carboxylates, which demonstrated that molecular design is an effective way to improve the electrochemical performances of organic material.[23]

Recently, sodium terephthalate $Na_2C_8H_4O_4$ ($Na_2TP$) is gaining extensive attention and has shown reliable electrochemical properties in terms of high sodium storage capacity, good cycling performance and rate capability. The first publication about $Na_2TP$ demonstrated a high reversible capacity of 250 mA h $g^{-1}$ and good cyclability,[24] resembling the crystal structure and electrochemical properties of lithium terephthalate ($Li_2C_8H_2O_6$, $Li_2TP$).[16] However, due to the intrinsic poor conductivity of organic materials, they usually suffer from poor rate capability for sodium storage.[20] In this paper, bare $Na_2TP$ was synthesized from low-cost terephthalic acid, which is commonly used as a precursor for the polyester PET. To improve the electron conductivity of bare $Na_2TP$, graphene was used to modify bare $Na_2TP$ *via* a freeze-drying technique, followed by heat treatment at mild temperature.[25] The physical properties and electrochemical performances of the sodium terephthalate@graphene ($Na_2TP@GE$) hybrid were systematically investigated.

## Experimental

### Materials preparation

Bare sodium terephthalate $Na_2C_8H_4O_4$ ($Na_2TP$) was prepared *via* a modified acid–base reaction based on the previous report.[26] Terephthalic acid was used as the starting material, which is available in abundance from the recycling of polyethylene

*Centre for Clean Energy Technology, School of Mathematical and Physical Sciences, University of Technology Sydney, NSW 2007, Australia. E-mail: Guoxiu.wang@uts. edu.au*

† Electronic supplementary information (ESI) available: Nuclear magnetic resonance data, thermogravimetric analysis and scanning electron microscopy. See DOI: 10.1039/c6ra11809g

terephthalate. In a typical procedure, 0.02 mol of terephthalic acid was added into 10 mL sodium hydroxide solution (0.066 mol) with deionized water gradually added up to 50 mL until the full dissolution of the $Na_2TP$. The aqueous solution was slowly evaporated to collect the $Na_2TP$ crystals, which were further purified with copious ice-cold ethanol and dried at 120 °C for 12 h in vacuum.

Graphene oxide (GO) was synthesized by a modified Hummer's method.[27] Typically, natural graphite flakes (1.0 g, Sigma-Aldrich), $NaNO_3$ (1.0 g), and $H_2SO_4$ (98 wt%, 48 mL) were mixed and stirred in an ice bath, and $KMnO_4$ (6 g) was slowly added into the mixture. After mixing for 30 min, the ice bath was removed and the mixture was further stirred for another 48 h. Next, distilled water (90 mL) was added under stirring, while the temperature rose to 60 °C. Finally, $H_2O$ (240 mL, 60 °C) was added, followed by the slow addition of $H_2O_2$ (15 mL, 30%). The final suspension was centrifuged, filtered and washed with water several times to obtain graphene oxide. The as-synthesized graphene oxide was dispersed into distilled water and sonicated for 2 h to form a homogeneous suspension of $GO/H_2O$.

$Na_2TP@GE$ hybrid was synthesized via a freeze-drying technique. Firstly, 30 mg $Na_2TP$ powder was added into 5 mL $GO/H_2O$ suspension (3.0 mg $mL^{-1}$) to form a transparent brownish solution, which underwent freeze-drying at $-80$ °C for 48 h until complete dryness. Afterwards, the as-synthesized powder was ground and sintered at 300 °C for 2 h in Ar. As $Na_2TP$ is highly soluble in water, the graphene content in the $Na_2TP@GE$ hybrid was determined by dissolving this composite in copious water and collection of the filtrate, which was further purified and dried in an oven overnight. The final graphene content was 22 wt%.

### Structural and physical characterization

The crystal structure and phase purity of the as-prepared materials were characterized by X-ray powder diffraction (XRD), nuclear magnetic resonance (NMR) and Fourier transform infrared spectroscopy (FTIR). XRD data were collected on a Siemens D5000 Diffractometer with Cu Kα radiation ($\lambda = 0.15405$ nm) in the $2\theta$ range of $10 \leq 2\theta \leq 60°$ at a scanning step of $0.02°$ $s^{-1}$. NMR spectra were recorded on an Agilent 500 spectrometer at room temperature. Samples were dissolved in $D_2O$ prior sealing in a 5 mm NMR tube. FTIR was carried out using a Nicolet Magna 6700 FT-IR spectrometer. All spectra were obtained using 4 $cm^{-1}$ resolution and 64 scans at room temperature. The thermal stability of bare $Na_2TP$ was

determined by thermogravimetric analysis (TG, TA Instruments) using an SDT 2960 simultaneous DTA/TGA analyzer from RT to 800 °C at a heating rate of 5 °C $min^{-1}$ in air. The morphologies were analyzed via field emission scanning electron microscopy (FESEM, Zeiss Supra 55VP).

### Cell assembly and electrochemical testing

The electrochemical tests of both bare $Na_2TP$ and $Na_2TP@GE$ hybrid versus sodium were carried out in coin cells assembled inside an argon-filled glove box (Unilab, Mbraun, Germany). The bare $Na_2TP$ electrodes were made from 55 wt% active materials, 30 wt% carbon black, and 15 wt% polyvinylidene fluoride (PVDF), while the $Na_2TP@GE$ hybrid electrode were prepared from 85 wt% active materials and 15 wt% PVDF. For each cell, the loading mass was about 1 mg $cm^{-2}$ and the electrolyte was a solution of 1 M $NaClO_4$ in a mixture of ethylene carbonate (EC) and propylene carbonate (EC : PC = 1 : 1 volume ratio), in which 5 vol% fluoroethylene carbonate (FEC) was added as the electrolyte additive. To exclude the capacity contribution of carbon materials to the total capacity of the electrode, background tests were carried out on bare carbon black and bare graphene, respectively. Both electrodes were made from 85 wt% carbon materials and 15 wt% PVDF. The charge–discharge tests were performed between 0.01–2.0 V on a Neware battery tester at various current densities.

## Results and discussion

The synthetic process of the $Na_2TP@GE$ hybrid architecture is shown in Scheme 1. First, the GO suspension was prepared via a modified Hummer's method. Second, the as-prepared $Na_2TP$ was added into the GO suspension according to the desired ratio. Afterwards, the $Na_2TP@GO$ suspension was frozen immediately after the full dissolution of $Na_2TP$ salts. Finally, the $Na_2TP@GE$ hybrid was obtained via the freeze-drying of the $Na_2TP@GO$ suspension, which has been reported beneficial for electrochemical performance,[28–30] followed by mild-temperature sintering. The phases of $Na_2TP$ and $Na_2TP@GE$ were characterized by XRD and are shown in Fig. 1(a) and (b), respectively. The XRD patterns of both samples unveil that $Na_2TP$ is single phase and has an orthorhombic structure, which can be indexed to the space group $P2_1/c$ with JCPDS card no. 00-052-2146.[31] As shown in Fig. 1, both XRD patterns resemble each other with the peak intensities of $Na_2TP@GE$ hybrid much lower than that of the bare $Na_2TP$, indicating the much smaller
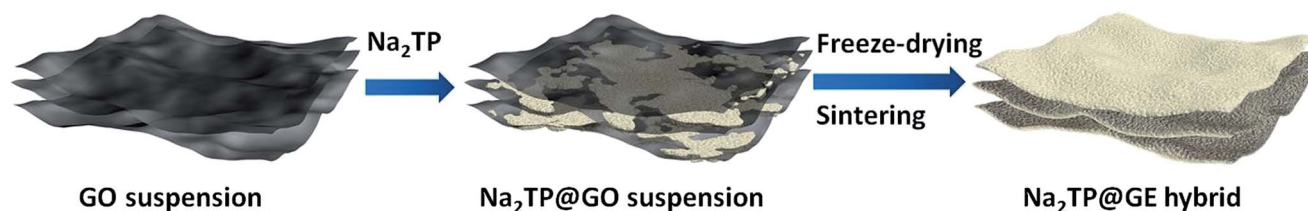


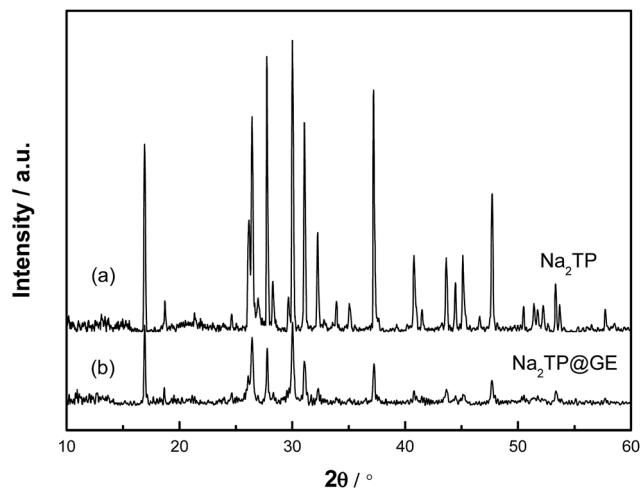**Scheme 1** Schematic illustration of the formation of $Na_2TP@GE$ hybrid.

Fig. 1   XRD of (a) bare $Na_2TP$ and (b) $Na_2TP@GE$ composite materials.

particle size of the hybrid than the bare sample. The structure of $Na_2TP$ is further confirmed by $^1H$ and $^{13}C$ NMR (Fig. S1†).

Fig. 2 compares the FTIR spectra of terephthalic acid, bare $Na_2TP$ and $Na_2TP@GE$. The broad peak at 940 cm$^{-1}$ corresponds to O–H bending vibrations of the carboxyl (COOH) group in the terephthalic acid raw material. After the synthetic reaction, it clearly shows the disappearance of O–H bend bond from the raw material, which has resulted from the sodium insertion into the molecule to form the disodium terephthalate. The absorption bands at 1394 and 1566 cm$^{-1}$ are attributed to the C–C stretching vibration from the aromatic structure. Meanwhile, the FTIR spectra of bare $Na_2TP$ and $Na_2TP@GE$ show the same peak positions, suggesting the subsequent graphene modification process does not affect the phase of $Na_2TP$. In addition, Fig. S2† displays the thermogravimetric analysis of bare $Na_2TP$, and demonstrates its high thermal stability with less than 1 wt% weight loss up to 500 °C in air. The morphology of bare $Na_2TP$ and $Na_2TP@graphene$ hybrids was revealed by FESEM imaging
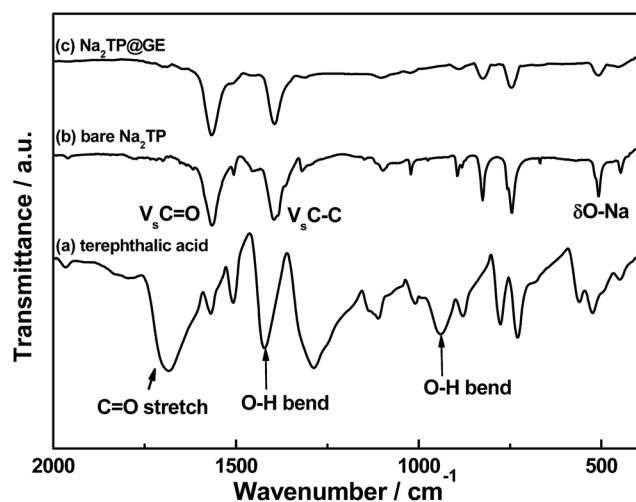
displayed in Fig. 3. In detail, Fig. 3(a) shows that the bare $Na_2TP$ exhibited irregular particles with a size in micrometre range. The high-magnification image in Fig. 3(b) reveals a flake-like structure of the bare $Na_2TP$ with tens of microns in size. On the contrary, the $Na_2TP@GE$ hybrid demonstrates a regular monolith structure with well-ordered multiple channels (Fig. 3(c)) achieved by the freeze-drying method. The zoom-in image of the white rectangular area of Fig. 3(c) is shown in Fig. 3(d) and it can be clearly seen that the ordered channels are interconnected. These channels are beneficial for the electrolyte penetration and electron transfer which will lead to much improved electrochemical properties when used as the electrode material in Na-ion battery applications. More FESEM images of the $Na_2TP@GE$ hybrid are shown in Fig. S3†, which further confirm its unique nanoarchitecture.

The electrochemical performances of both bare $Na_2TP$ and $Na_2TP@GE$ were tested in a voltage range of 0.01–2 V vs. $Na^+/Na$ at different current densities. Cycling performances of pristine carbon black and graphene are shown in Fig. S4† as the background tests.

All the electrochemical properties of bare $Na_2TP$ and $Na_2TP@GE$ hybrid were calculated based only on the weight percentage of organic material in each electrode. Discharge curves for the 2$^{nd}$, 100$^{th}$, 250$^{th}$ and 500$^{th}$ cycles are shown in Fig. 4(a) and (b), respectively. Both samples displayed similar charge–discharge profiles with the potentials dropping dramatically to reach a plateau of around 0.29 V, which are related to the desodiation of sodium ions from $Na_2TP$,[24] indicating that the presence of graphene did not affect the reaction mechanism of $Na_2TP$. Theoretically, the reaction mechanism of sodium terephthalate vs. sodium can be expressed as $Na_2C_8H_4O_4 \xleftrightarrow{2Na^+ + 2e^-} Na_4C_8H_4O_4$ with the two carbonyl groups allowing for the intercalation and deintercalation of two Na ions into its molecular structure, resulting in a specific capacity of 255 mA h g$^{-1}$. In the first cycles, it is noticeable that both bare $Na_2TP$ and $Na_2TP@GE$ produced large irreversible capacity loss.
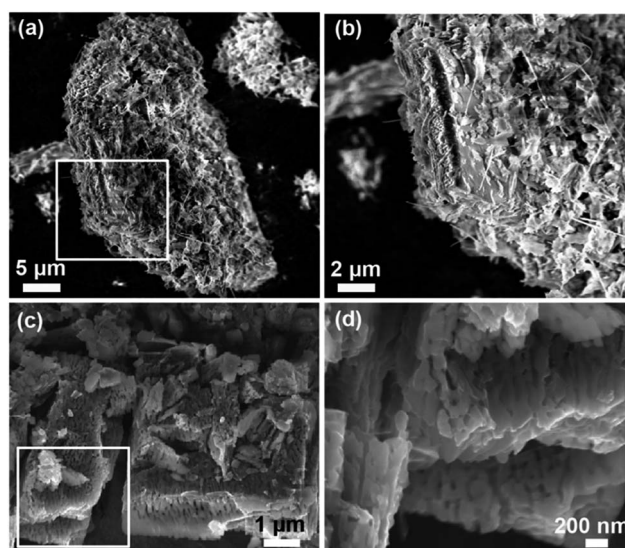


Fig. 2   FTIR spectra of (a) terephthalic acid, (b) bare $Na_2TP$ and (c) $Na_2TP@GE$ hybrid.



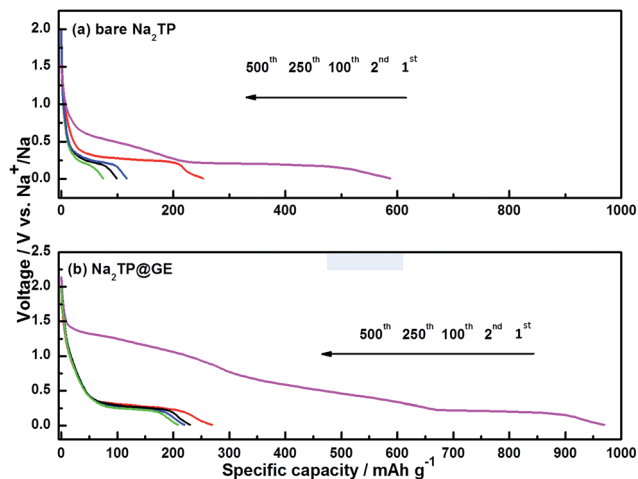Fig. 3   FESEM images of (a), (b) bare $Na_2TP$ and (c), (d) $Na_2TP@GE$ hybrid at different magnifications.

**Fig. 4** Discharge profiles of (a) bare $Na_2TP$ and (b) $Na_2TP@GE$ hybrid at selected cycle numbers at a current density of 100 mA $g^{-1}$.



**Fig. 5** Cycling performances of bare $Na_2TP$ (circle) and $Na_2TP@GE$ hybrid (triangle) for 500 cycles (corresponding coulombic efficiencies shown in the inset).



**Fig. 6** Rate performances of bare $Na_2TP$ and $Na_2TP@GE$ hybrid at various current densities.

This is related to the irreversible decomposition of the electrolytes to form solid electrode interface (SEI) resulting relatively low coulombic efficiencies in the first cycle. At the $2^{nd}$ cycle, the discharge capacities of bare $Na_2TP$ and $Na_2TP@GE$ are 253.5 mA h $g^{-1}$ and 268.9 mA h $g^{-1}$, respectively, which are close to the theoretical capacity of $Na_2TP$. During the subsequent cycles, the specific capacity of bare $Na_2TP$ decays dramatically, while the $Na_2TP@GE$ hybrid exhibited outstanding cyclability, delivering much higher discharge capacities than those of the bare $Na_2TP$. To be specific, at the $250^{th}$ cycle, the $Na_2TP@GE$ hybrid electrodes delivered a discharge capacity of 219.7 mA h $g^{-1}$, which is much higher than the discharge capacity of bare $Na_2TP$ (98.97 mA h $g^{-1}$) and previous reports.[21,24] It should be noted that during the following charge–discharge process, the discharge profiles of $Na_2TP@GE$ composite traced back very well and showed excellent reversibility, suggesting fast electron transfer in the $Na_2TP@GE$ materials. On the contrary, the discharge voltage plateau of bare $Na_2TP$ was decreasing while cycling, revealing the large polarization and poor reversibility of this material.

Fig. 5 further compares the cycling performances and their corresponding coulombic efficiencies of bare $Na_2TP$ and $Na_2TP@GE$ hybrid. The $Na_2TP@GE$ hybrid electrode showed to have much higher coulombic efficiency than that of the bare $Na_2TP$. However, both samples coulombic efficiencies are still quite low compared with the conventional Li-ion batteries. This might be related to the side reactions involved during the electrochemical process in the Na-ion battery system, which needs to be further improved. After 500 cycles, 77.3% of the $Na_2TP@GE$ hybrid electrode's initial capacity (207.9 mA h $g^{-1}$) was found to be retained, compared to 29.3% (74.3 mA h $g^{-1}$) of the initial bare $Na_2TP$ capacity, indicating the $Na_2TP@GE$ hybrids are highly reversible towards sodium insertion. The rate performances of bare $Na_2TP$ and $Na_2TP@GE$ are evaluated based on the profile of the charge–discharge current densities shown in Fig. 6.

At a low current density of 100 mA $g^{-1}$, there is less difference in discharge capacity between both samples. However,
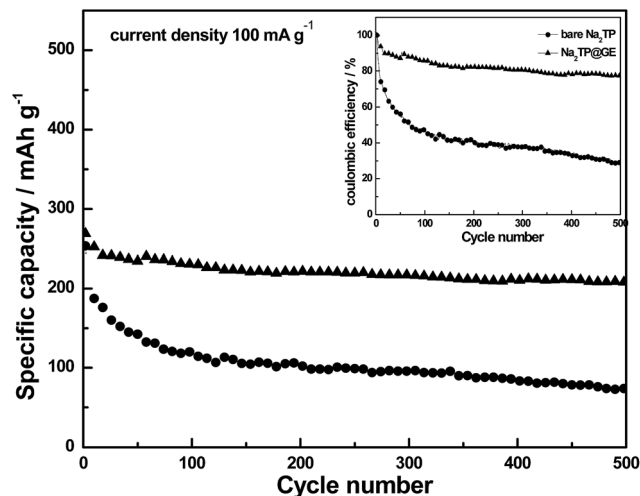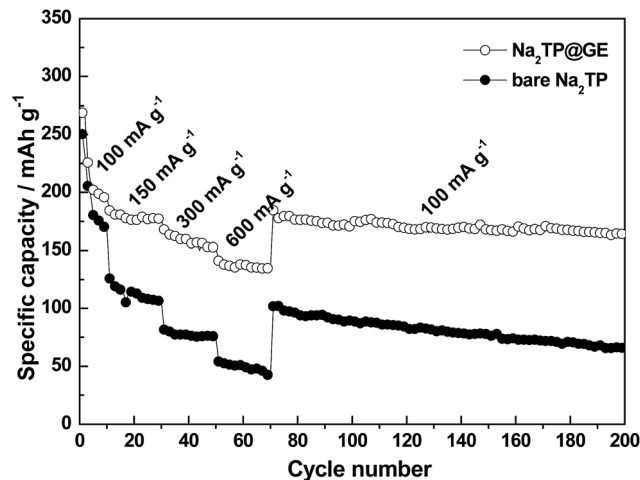
when the current densities are increased to 300 mA $g^{-1}$, the composite electrode delivered twice the discharge capacity of the bare one, with the values of 168 mA h $g^{-1}$ and 81.5 mA h $g^{-1}$, respectively. Even at a high current density of 600 mA $g^{-1}$, the $Na_2TP@GE$ hybrid electrodes were still able to maintain a reversible discharge capacity of 141 mA h $g^{-1}$, while the bare electrode only reached less than 54 mA h $g^{-1}$. It is worth noting that when the cells continued cycling at the original low current density of 100 mA $g^{-1}$, the hybrid electrodes recovered well and delivered a capacity of around 184.6 mA h $g^{-1}$.

## Conclusions

The $Na_2TP@GE$ hybrid was prepared by a freeze-drying method. FESEM analysis confirmed that $Na_2TP@GE$ hybrid showed a well-constructed multi-channelled structure, with well

retained graphene layers after freeze-drying. The electro-chemical properties of both bare $Na_2TP$ and $Na_2TP@GE$ hybrid have been fully evaluated through a series of electrochemical tests. The hybrid electrode delivered a high reversible capacity of 268.9 mA h $g^{-1}$, and high capacity retention of 77.3% after 500 cycles. In addition, at elevated cycling current densities, the $Na_2TP@GE$ hybrid exhibits more than twice the reversible capacities of the bare one. The improved electrochemical performances of $Na_2TP@GE$ can be ascribed to its unique nanoarchitecture with multi-channelled monolithic grains beneficial for fast intercalation of sodium ions during the pro-longed charge–discharge process. The graphene layers main-tain well separated *via* freeze-drying, which leads to synergetic effects in preventing particle agglomeration, enhancing elec-tronic conductivity of the insulating $Na_2TP$, while maximizing reaction sites for electrochemical reactions. The $Na_2TP@GE$ hybrid is a promising organic hybrid material for high-performance Na-ion batteries.

## Acknowledgements

## References and notes

1 M. D. Slater, D. Kim, E. Lee and C. S. Johnson, *Adv. Funct. Mater.*, 2013, **23**, 947–958.

2 S.-W. Kim, D.-H. Seo, X. Ma, G. Ceder and K. Kang, *Adv. Energy Mater.*, 2012, **2**, 710–721.

3 D. Kundu, E. Talaie, V. Duffort and L. F. Nazar, *Angew. Chem., Int. Ed.*, 2015, **54**, 3431–3448.

4 X. Xiang, K. Zhang and J. Chen, *Adv. Mater.*, 2015, **27**, 5343–5364.

5 R. Alcantara, J. M. Jimenez-Mateos, P. Lavela and J. L. Tirado, *Electrochem. Commun.*, 2001, **3**, 639–642.

6 S. Wenzel, T. Hara, J. Janek and P. Adelhelm, *Energy Environ. Sci.*, 2011, **4**, 3342–3345.

7 L. Baggetto, J. K. Keum, J. F. Browning and G. M. Veith, *Electrochem. Commun.*, 2013, **34**, 41–44.

8 B. Farbod, K. Cui, W. P. Kalisvaart, M. Kupsta, B. Zahiri, A. Kohandehghan, E. M. Lotfabad, Z. Li, E. J. Luber and D. Mitlin, *ACS Nano*, 2014, **8**, 4415–4429.

9 L. Wu, H. Lu, L. Xiao, J. Qian, X. Ai, H. Yang and Y. Cao, *J. Mater. Chem. A*, 2014, **2**, 16424–16428.

10 Y. Zhao and A. Manthiram, *Chem. Mater.*, 2015, **27**, 3096–3101.

11 D. L. Williams, J. J. Byrne and J. S. Driscoll, *J. Electrochem. Soc.*, 1969, **116**, 2.

12 X. Han, C. Chang, L. Yuan, T. Sun and J. Sun, *Adv. Mater.*, 2007, **19**, 1616.

13 Z. Song, Y. Qian, M. L. Gordin, D. Tang, T. Xu, M. Otani, H. Zhan, H. Zhou and D. Wang, *Angew. Chem., Int. Ed.*, 2015, **54**, 13947–13951.

14 X. Wu, J. Ma, Y.-S. Hu, H. Li and L. Chen, *J. Energy Chem.*, 2014, **23**, 269–273.

15 L. Fedele, F. Sauvage and M. Becuwe, *J. Mater. Chem. A*, 2014, **2**, 18225–18228.

16 M. Armand, S. Grugeon, H. Vezin, S. Laruelle, P. Ribiere, P. Poizot and J. M. Tarascon, *Nat. Mater.*, 2009, **8**, 120–125.

17 H. Chen, M. Armand, M. Courty, M. Jiang, C. P. Grey, F. Dolhem, J.-M. Tarascon and P. Poizot, *J. Am. Chem. Soc.*, 2009, **131**, 8984–8988.

18 H. Chen, M. Armand, G. Demailly, F. Dolhem, P. Poizot and J. M. Tarascon, *Chemsuschem*, 2008, **1**, 348–355.

19 S. Renault, J. Geng, F. Dolhem and P. Poizot, *Chem. Commun.*, 2011, **47**, 2414–2416.

20 J. Geng, J.-P. Bonnet, S. Renault, F. Dolhem and P. Poizot, *Energy Environ. Sci.*, 2010, **3**, 1929–1933.

21 A. Abouimrane, W. Weng, H. Eltayeb, Y. Cui, J. Niklas, O. Poluektov and K. Amine, *Energy Environ. Sci.*, 2012, **5**, 9632–9638.

22 S. Wang, L. Wang, Z. Zhu, Z. Hu, Q. Zhao and J. Chen, *Angew. Chem., Int. Ed.*, 2014, **53**, 5892–5896.

23 C. Wang, Y. Xu, Y. Fang, M. Zhou, L. Liang, S. Singh, H. Zhao, A. Schober and Y. Lei, *J. Am. Chem. Soc.*, 2015, **137**, 3124–3130.

24 L. Zhao, J. Zhao, Y.-S. Hu, H. Li, Z. Zhou, M. Armand and L. Chen, *Adv. Energy Mater.*, 2012, **2**, 962–965.

25 C. Luo, Y. Zhu, Y. Xu, Y. Liu, T. Gao, J. Wang and C. Wang, *J. Power Sources*, 2014, **250**, 372–378.

26 Y. Park, D.-S. Shin, S. H. Woo, N. S. Choi, K. H. Shin, S. M. Oh, K. T. Lee and S. Y. Hong, *Adv. Mater.*, 2012, **24**, 3562–3567.

27 W. S. Hummers and R. E. Offeman, *J. Am. Chem. Soc.*, 1958, **80**, 1339.

28 S. Renault, V. A. Mihali and D. Brandell, *Electrochem. Commun.*, 2013, **34**, 174–176.

29 L. Fédèle, F. Sauvage, J. Bois, J.-M. Tarascon and M. Bécuwe, *J. Electrochem. Soc.*, 2014, **161**, A46–A52.

30 V.-A. Oltean, S. Renault, M. Valvo and D. Brandell, *Materials*, 2016, **9**, 142.

31 J. A. Kaduk, *Acta Crystallogr., Sect. B: Struct. Sci.*, 2000, **56**, 474–485.